High Performance Compact Multilayer Circular Spiral Inductors in Advanced Photoimageable Technology

Kamal K. Samanta, *Senior Member, IEEE*, and Ian D. Robertson, *Fellow, IEEE*

***Abstract*—This paper presents the development and thorough analysis of a wide range of coplanar-waveguide circular spiral inductors with remarkably high performance and inductance density using advanced multilayer (ML) photoimageable thick-film (Pimage-TF) multichip module (MCM) technology. The performances of the embedded spiral inductors are thoroughly analyzed, modeled, and compared with the competitive MCM technologies and are superior to most of the published results. A new design and layout generation technique with a simplified closed form expression for circular spiral inductors is proposed. Moreover, the impact of MCM/system-on-package technologies on inductor key parameters has been explained in detail and compared with other technologies. The cost-effective Pimage-TF-based inductors demonstrate the highest level of self-resonance frequency, as well as inductance density (15 nH/mm^2) reported to date in conventional thick-film-based ML MCM technologies, including low temperature cofired ceramic.**

***Index Terms*—Miniaturized inductor, multichip modules (MCM), mutilayer (ML) passive components, photoimageable.**

I. Introduction

EVER growing demands and emerging applications of microwave and millimeter-wave frequencies require the development of high performance and compact front-end architectures at a low cost. In a multichip module (MCM) or system-on-package (SOP), a number of RF front-end building blocks often require off-chip lumped elements, which cannot be incorporated on-chip with required quality. Among the passive components, the inductor is one of the key components determining the performance of many high-frequency circuits. The design of embedded inductors in a multilayer (ML) MCM/SOP environment with compact size, high self-resonance frequency (SRF), and good quality factor (Q) is very critical and requires intensive 3-D electromagnetic simulation. Spiral inductors are used to realize high-value inductance (>1 nH) [1]. The performance of a coplanar waveguide (CPW) circular spiral inductor is superior to that of a square or rectangular spiral with bend discontinuities and couplings at the corners [2]. Yet, in most of the reported ML MCM/SOP technologies, square spiral is used due to its easier layout version for design and optimization of performance in 3-D em simulator.

At the same time, in most of the commercially available 3-D em simulators (like HFSS) it is very difficult to draw the layout of a circular spiral. The circular spiral inductor is a technique of forming a planar inductor in a small space. The shape is described by an increasing radius with an angle. The most common type of spirals has radius functions and the equations used to algorithmically generate the spiral inductor layout are

$$R = R_i + k\theta \quad \text{Archimedes spiral} \quad (1)$$

$$R = R_i e^{h\theta} \quad \text{Logarithmic spiral} \quad (2)$$

$$R = \frac{R_i}{1.0 + kR_i\theta} \quad \text{Hyperbolic spiral} \quad (3)$$

where R_i and R_0 represent the inner radius and the outer radius of the inductor, respectively. Due to the nature of the circular spiral structure, it is not straightforward either to draw a quick layout for em simulation or to decide the total length, which is key to model other parameters of an inductor.

Further, in most of the reported cost-effective MCM technologies (except costlier thin-film-based MCM-D, deposition technology), including laminate (L), ML organic (MLO), and low temperature cofired ceramic (LTCC) [3]–[9], there are limitations in realizing fine conductor geometries. Due to that, either the size of an inductor becomes large or miniaturization is achieved mostly by exploring the ML capability, which introduce parasitics, reducing SRF, and hence frequency of operation [8], [10]. This causes difficulties in realizing high-value inductance with high SRF. For a ML inductor, a large area is occupied by the buried vias, whereas keeping the footprint on the surface layer minimizes the dielectric loss due to propagation of part of the fields in the air [9]. Thus, to optimize the performance of an inductor, modern photoimageable thick-film (Pimage-TF) technology with thin dielectric layer and fine conductor geometries, as well as thick metallization, has been demonstrated as highly suitable [5], [11]. This advanced process is cost-effective, straightforward, and compatible with many fabrication processes, including LTCC. The process has been used to realize high performance ceramic-based various transmission lines, a wide

Manuscript received December 3, 2013; revised August 20, 2014; accepted September 16, 2014. Date of publication November 3, 2014; date of current version December 5, 2014. Recommended for publication by Associate Editor D. G. Kam upon evaluation of reviewers' comments.

K. K. Samanta is with Milmega/AMETEK Ltd., Ryde PO33 2BE, U.K., and also with the School of Electronic and Electrical Engineering, Institute of Microwaves and Photonics, University of Leeds, Leeds LS2 9JT, U.K. (e-mail: kksamanta@ieee.org).

I. D. Robertson is with the School of Electronic and Electrical Engineering, Institute of Microwaves and Photonics, University of Leeds, Leeds LS2 9JT, U.K. (e-mail: i.drobertson@leeds.ac.uk).

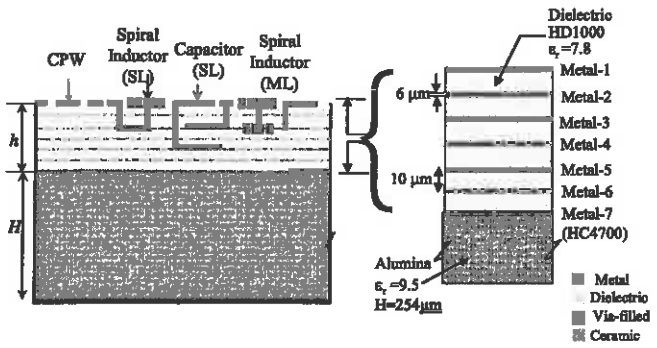

Fig. 1. Cross-sectional view of the six layer process used for integrated passive components (SL and ML) in ML advanced Pimage-TF MCM/SOP technology.

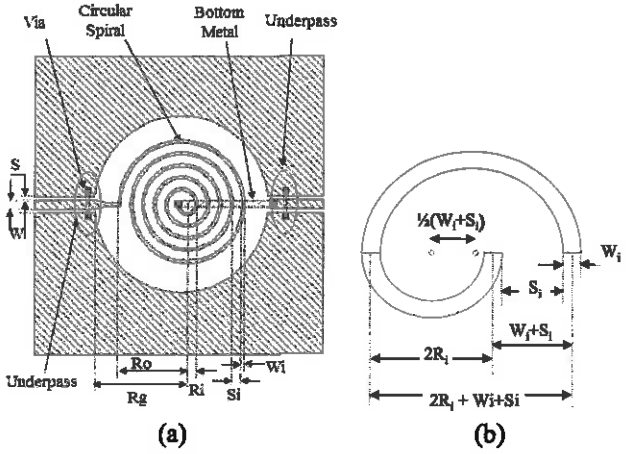

Fig. 2. (a) Top schematic of a ML CPW-based circular spiral inductor with five turns. (b) Enlarged subsectional view.

range of lumped and passive components and circuits up to 110 GHz [11]–[16], including development of a highly compact MCM receiver at 60 GHz [5]. Furthermore, the technology is being demonstrated, as a highly suitable approach, to realize cost-effective microwave and millimeter-wave MCM and SOP modules [5], [15].

Here, a large number of CPW planar circular spiral inductors are developed, characterized, and modeled on ML Pimage-TF MCM technology with remarkably high performance, miniaturization and up to very high value of inductance as well as SRF. A simplified layout generation technique, without use of any computational methods [16], and closed form expressions have been proposed for EM/layout-based design of a circular spiral inductor. Furthermore, for the first time, the impact of different conventional MCM technologies on the CPW spiral inductor's key parameters has been detailed, the reported highest performances are compared, and the superiority of the proposed technology has been demonstrated.

II. Theoretical Analysis and Closed-Form Expression

The test structures were fabricated in photoimageable advanced thick-film technology [11], [12] on a ceramic (Alumina) base substrate (CoorsTek ADS-96R) using a conventional off-contact screen printer. A cross-sectional view of the six layer process used for integrated passive components is shown in Fig. 1. Layers of photoimgeable dielectric paste (HD1000) and low-loss silver conducting paste (HC4700) were printed alternately using screen printing technique.

A. Derivation of Novel Closed-Form Expression

As shown in Fig. 2, R_i, S_i, W_i, and R_g are the inner radius, line space, line widt h, and the center to the ground plane radius, respectively. The inductors have been constructed by a number of semicircles with increasing radius and toggling the center between two points, which are separated by inner radius (R_i). The diameter of the first semicircle of the first turn is

$$D_{\text{nm}} = D_{11} = 2R_i. \tag{4}$$

Here, n corresponds to the number of turns and m is to represent the first ($m = 1$) or the second ($m = 2$) semicircular trace of a turn.

Diameter for the second half cycle of the first turn ($n = 1$, $m = 2$) can be written as

$$D_{12} = 2R_i + (S_i + W_i). \tag{5}$$

Likewise, the diameter of the first semicircle of second turn, can be expressed as

$$D_{21} = 2R_i + 2\,(S_i + W_i)\,. \tag{6}$$

Similarly, for N turns there are $2 \times N$ semicircular traces and the total length can be written as

$$l = \pi\,[2R_i + \{2R_i + (S_i + W_i)\} + \{2R_i + 2\,(S_i + W_i)\} + \cdots + 2R_{2N-2} + 2R_0]\,. \tag{7}$$

Here, the last term gives the highest radius (R_o), which is the second semicircle of the Nth turn and can be expressed as

$$R_o = R_{2N} = R_i + \frac{1}{2}(2N - 1)(S_i + W_i). \tag{8}$$

For, $n = 2(N) - 1$

$$R_o = R_i + \frac{1}{2}n(S_i + W_i) \tag{9}$$

and

$$l = \pi[2R_i \times 2N + (W_i + S_i)(1 + 2 + 3 + \cdots + n)]$$
$$\text{or, } l = \pi[4R_i \times N + N(2N - 1)(W_i + S_i)]. \tag{10}$$

Furthermore, for an N turns coil with conductor to ground gap of W_g and the center of the coil to the ground plane radius R_g from (7) can be written as

$$R_g = R_i + \frac{1}{2}n(S_i + W_i) + W_g. \tag{11}$$

From (10), one can get accurate length of the trace of a circular spiral inductor from inner radius (R_i), spacing (S_i) and width (W_i) of the conductor track and the same can be used for the layout generation and EM-based design and optimization of an inductor performance in a ML MCM circuit.

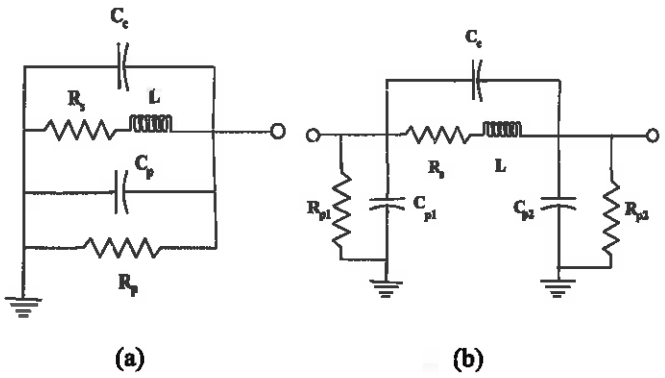

Fig. 3. Equivalent lumped element circuit models for a CPW circular spiral inductor on ML ceramic substrate. (a) One-port circuit model. (b) Two-port circuit model.

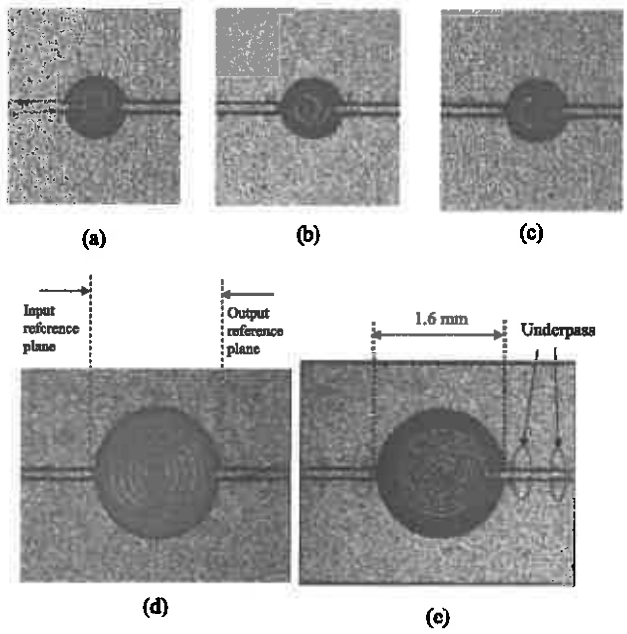

Fig. 4. Microphotographs of some of the fabricated compact coplanar circular spiral inductors in advanced photoimageable technology with different turns and layers for (a) loop, (b) 1.5T on SL, (c) 1.5T on DL, (d) 5T, and (e) 8T.

B. Parameter Extraction

The one-port lumped element equivalent circuit model and the two-port circuit model for the inductors on the ML MCM are shown in Fig. 3, whereas Fig. 4 shows the microphotograph of some of the fabricated CPW circular spiral inductors fabricated on a ML photoimageable substrate. In the circuit, R_s models the metal trace resistance, L presents the inductance, and C_c, C_{p1}, and C_{p2} models capacitive coupling effects. C_c models the coupling between turns of the coil and C_{p1} and C_{p2} represent the parasitic coupling between the coil and the surrounding ground at the input and the output, respectively. Here, the input is connected with an underpass, and the output is on the top layer. Due to the presence of the underpass, C_{p2} is considerably different from C_{p1} for a low-value inductor.

From the circuit model, the effective impedance is represented in terms of circuit parameters as

$$\frac{1}{Z_{\text{in}}(\omega)} = \frac{1}{R_s + j\omega L} + j\omega(C_{p1} + C_c). \tag{12}$$

The series resistance (R_s) and the equivalent inductance (L_e) of the spiral inductor, derived from the input impedance are

$$R_s(\omega) = \text{Re}(Z_{\text{in}}) \tag{13}$$

$$L_e(\omega) = \frac{\text{Im}(Z_{\text{in}})}{2\pi f}. \tag{14}$$

Again, from the admittance parameters we can find the series inductance (L)

$$L(\omega) = \text{Im}\left(\frac{-Y_{12}}{2\pi f}\right). \tag{15}$$

For the circular spiral inductor, the series inductance (L) and the equivalent inductance (L_e), which is the effective inductive reactance due to parasitics, can be extracted from the two-port S-parameters.

The series resistance (R_s) is calculated with the equations of skin effect resistance of the equivalent rectangular conductor and can be expressed as [6]

$$R_s = \frac{K R_{\text{sh}} l}{2W_i} \quad \text{Ohm} \tag{16}$$

where, R_{sh} is the sheet resistance of the trace (Ω/sq), $K = 1.5$ empirically, W_i is the width of the coil, and l is the total length of the inductor.

III. Inductor Fabrication and Measurement Results

Inductors are realized for different turns and inductance. For an N turns inductor, the structure was designed using incremental radius of $2N$ semicircular traces of diameters calculated from (4) and (5). The outer radius (R_o) and the center to the ground plane radius (R_g) were calculated from (9) and (11), respectively. To avoid the influence of the ground plane on the inductor value, the track to ground gap (W_g) is kept large. The initial values of inductance were estimated using the closed form (10) and the EM simulator and accordingly the inner radius (R_i), strips width (W_i), and slots width (S_i) were optimize. For different inductors, the physical dimensions and some of the major parameters have been shown in Table I. In a CPW structure, parasitic is less due to negligible substrate capacitance. Moreover, the gap between turns was increased ($\sim$100 μm) to reduce the coupling capacitance, and to optimize the size, the track width (W_i) was set to 20 μm.

The two-port S-parameters for the lumped elements were measured using an HP8510XF vector network analyzer and cascade microtech coplanar ground–signal–ground probes of 100-μm pitches. The parameters were extracted based on measurement data for different CPW inductors, fabricated in the ML-thick-film process. The deembedded S-parameters were used for parameter extraction. The variation of extracted C_{p1} with frequency for a loop, single turn (1T), 1.5 turns

TABLE I

PHYSICAL DIMENSIONS AND MAJOR PARAMETERS FOR THE INDUCTORS

Coil Type	Tu rns (n)	Parameters (μm)				f_{Qmax} GHz	SRF GHz	Q_{max}
		R_i	W_i	S_i	Leng (l)			
Loop	-	135	20	-	1060	16	>40	>110
Single layer	1	100	20	110	835	15.1	32.5	105
Single layer	1.5	100	20	110	1555	10.6	20.5	82
Double layer	1.5	100	20	110	1555	10.3	19.5	80
Single layer	5	100	20	110	12330	1.6	2.7	35
Single layer	8	100	20	60	20106	1.2	2	31

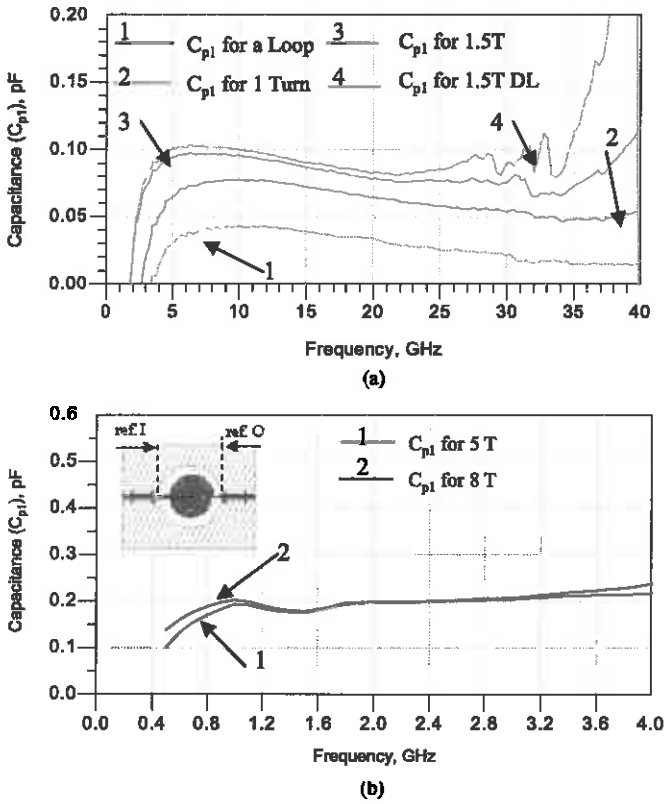

Fig. 5. Measured parallel ground parasitic capacitance (C_{p1}) for (a) loop, 1T, 1.5T, and 1.5T DL inductors and (b) 5T and 8T inductors on ML photoimageable MCM/SOP substrate.

single layer (SL) (1.5T), 1.5 turns (1.5T DL), 5 turns (5T), and 8 turns (8T) inductors, are shown in Fig. 5(a) and (b), respectively, whereas Fig. 6(a) and (b) compares the extracted difference between C_{p1} and C_{p2} for 1T and 5T inductors. This captures the asymmetry of the structure due to the presence of the underpass. However, this difference is not significant in the case of a loop, due to its planar structure, and also for

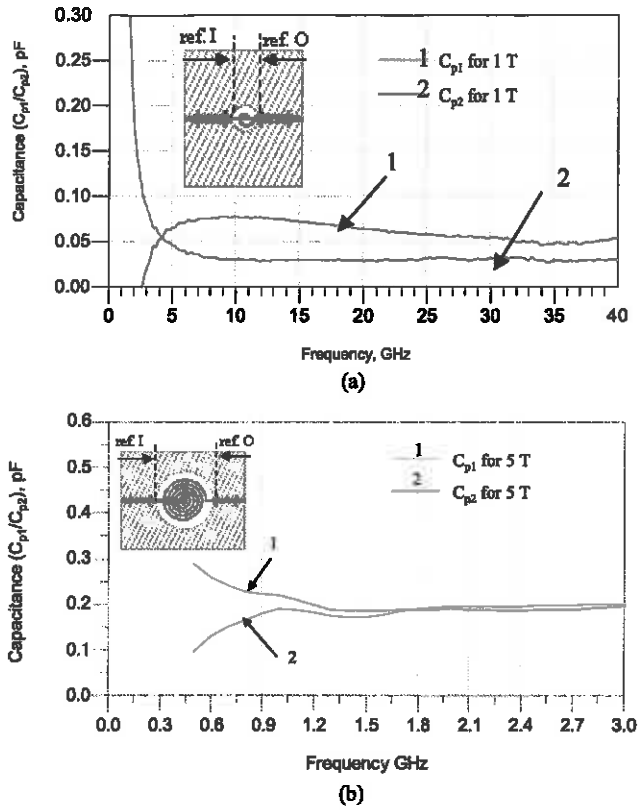

Fig. 6. Measured parallel ground parasitic capacitances, C_{p1} and C_{p2}, for (a) 1T and (b) 5T CPW circular spiral inductor on a ML MCM/SOP substrate.

the high value inductors. For the 5T inductor, due to its large track area, the total C_p is much larger than the contribution due to underpass, as shown in Fig. 6(b). Fig. 7(a) and (b) compares the measured and modeled magnitude and phase of S_{11} for the 5T CPW circular spiral inductor on ML MCM. A comparison of the tested performances for the 1.5T SL and double layer (DL) inductors are presented in Fig. 8. This shows that toward low frequency the inductances (L/Le) are similar for both of the inductors, but the parasitic coupling capacitance (C_{p1}) is higher in DL inductor than that in a SL inductor. In a DL inductor, fields are more confined inside dielectric, whereas in a SL a part of the fields propagates in the air. Thus, a DL structure suffers from additional dielectric loss and also losses from a large number of buried interlayer interconnecting vias. For the DL inductor, due to increase in parasitics, with frequency the inductive reactance changes more rapidly and hence provides a lower SRF than that for the SL inductor.

The physical dimensions and major parameters for different inductor geometries are listed in Table I. As the size of a inductor increases from loop to 8T, the inductance (L) increases from 0.6 to 31 nH, whereas the Q and SRF decrease from >110 to 30 and >40 to 2 GHz, respectively. The comparison between the extracted (measured) and simulated inductance (L) and (L_e) for 5T and 8T inductors are shown in Figs. 9 and 10, respectively. Fig. 11 compares the measured and the modeled inductance (L) for the inductors with various turns (1T, 1.5T, 5T, and 8T), whereas the extracted and the

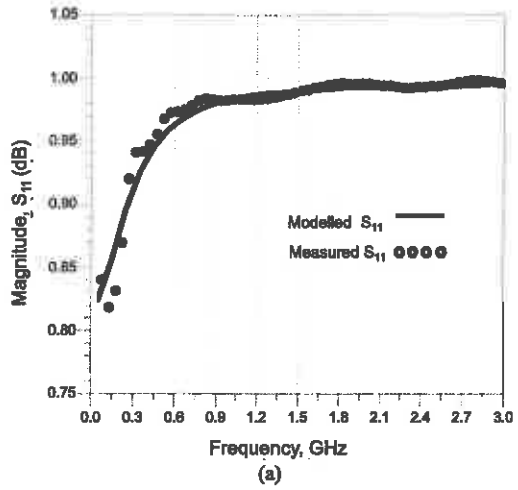

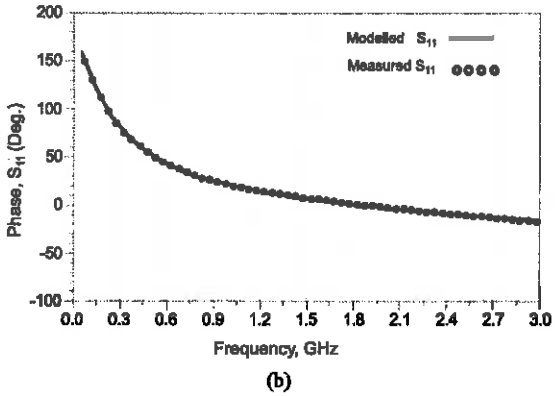

Fig. 7. Measured and modeled S_{11} of the CPW circular spiral inductor in ML MCM. (a) Magnitude plots of S_{11}. (b) Phase plots of S_{11} (deg).

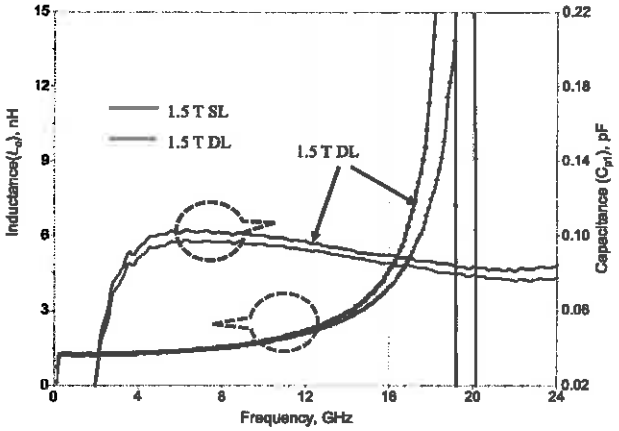

Fig. 8. Comparison of the performances for the 1.5T SL and DL inductors.

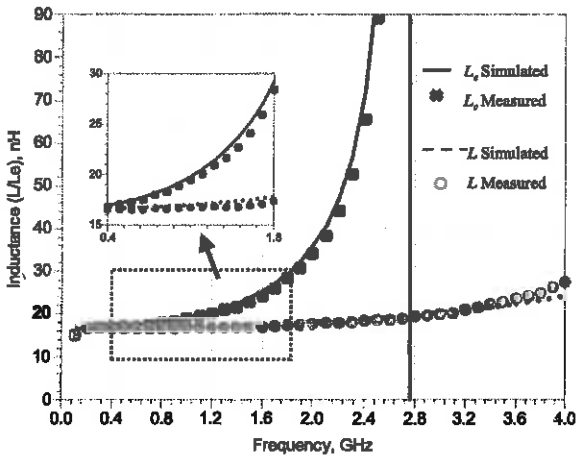

Fig. 9. Comparison of measured and simulated equivalent inductance (L_e) and series inductance (L) for a compact 5T CPW spiral inductor in advanced ML-thick-film technology.

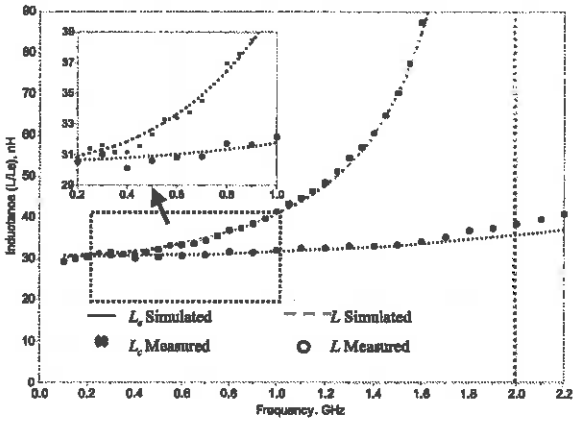

Fig. 10. Comparison of measured and simulated equivalent inductance (L_e) and series inductance (L) for a highly compact 8T CPW spiral inductor in advanced ML-thick-film technology.

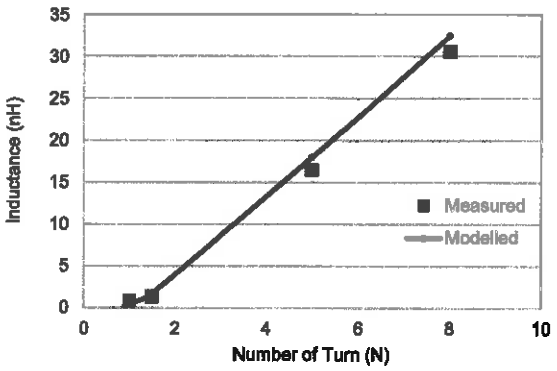

Fig. 11. Comparison of measured and modeled inductance (L) for various turns (1T, 1.5T, 5T, and 8T).

modeled S_{11} for 5T and 8T inductors have been compared in Fig. 12. From these results, a good agreement is observed between the model and the measurement. At the same time, as shown in the microphotographs (Fig. 4) the coil size for the 31 nH inductor is only 1.6 mm × 1.6 mm × 0.7 mm, which demonstrates one of the highest levels of miniaturization and inductance value ever reported in a conventional thick-film-based MCM technology. The lumped-element modeled parameters, R_s, C_{p1}, C_{p2}, and L, for various inductors, are listed in Table II. Presented results demonstrate that using the new layout generation technique and the closed form equation high quality circular spiral inductors can be realized on advanced ML-thick-film ceramic-based substrate with high miniaturization and SRF.

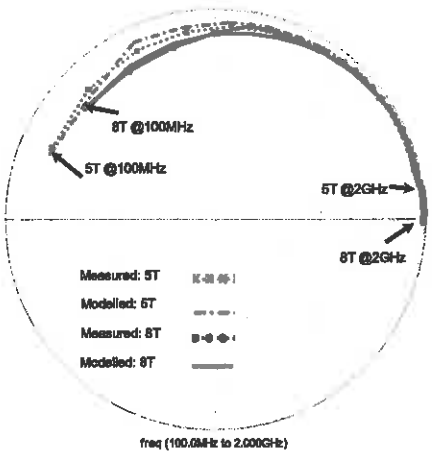

Fig. 12. Measured and modeled S_{11} for 5T and 8T inductors.

TABLE II
LUMPED-ELEMENT MODEL PARAMETERS FOR THE INDUCTORS

D. No.	Coil Type	Turns	L (nH)	C_{p1} (pF)	C_{p2} (pF)	C_c (pF)	R_s (Ω)
1	*Loop*	-	0.7	0.02	0.02	-	0.4
2	*Single layer*	1	0.8	0.07	0.035	0.001	0.5
3	*Single layer*	1.5	1.3	0.083	0.05	0.009	1.4
4	*Double layers*	1.5	1.3	0.085	0.055	0.01	1.25
5	*Single layer*	5	16.5	0.21	0.19	0.03	4.2
6	*Single layer*	8	30.6	0.22	0.21	0.04	6

IV. PERFORMANCE COMPARISON WITH OTHER TECHNOLOGIES

A. Technology Impact on Multilayer MCM/SOP Inductor Performance

In most of the reported MCM techniques (MCM-L, LTCC, MLO, and LCP) due to limitations on the conductor geometric resolution, high-value inductances are realized by distributing inductor track in multiple layers [3]–[9]. For a multiple layered (>2 layers) inductor, large area is occupied by the buried vias, whereas a planar structure keeping the footprint on the surface layer, minimizes the dielectric loss due to part of the fields' propagation in the air [9]. The inner radius (R_i), line width (W_i), separation between turns (S_i), and number of turns (n) are the main physical parameters determining the value of an inductor. The length (l) is the most important determinant of inductance value, which is followed by the line width (W_i). For a practical structure, inductance is weakly dependent on metal thickness. For same inductance value, a wider inductor requires a longer length than that for a narrower one.

In general, the technology which provides thinner metal is associated with a narrower width compared with those which offer thicker metal. The tradeoff is that the inductor with a large conducting cross section will provide a low resistance (R_s); consequently a better Q, but due to its large footprint, parallel ground capacitance, C_p, is larger, leading to a lower SRF. The proposed advanced thick-film technology, with its special kind of material and in combination with advanced fabrication process, can provide a thick metal layer as well as a narrow track width. Therefore, this technology offers a unique potential to realize a very high-value inductor on the surface layer (like in thin film technology), yet providing a much higher SRF and compactness as well as the inductance value, compared with most of the conventional thick-film MCM/SOP technologies reported so far. After considering the shrinkage in the design stage, the effect of process variation on metal-thickness and line-width might not have significant influence on a spiral inductor.

B. MCM/SOP Technologies and Comparison of Inductors Performance

Comparisons of compactness and some of the achieved highest performances for inductors in different MCM technologies, including MCM-L (laminate), LTCC, LCP, MLO, and Pimage-TF are shown in Tables III and IV. Table III compares different parameters, including compactness, in terms of inductance (nanohenry) per foot-print area (on the surface layer, mm^2), and the highest inductance value (L) achieved in different technologies. This clearly demonstrates that the highest value inductor, 31 nH, with a highest inductor density, 15 nH/mm^2, can be achieved in Pimage-TF technology. This compactness is shown better than those reported in laminate and MLO technologies. In LTCC, with conventional thick-film technology even a medium value inductor (16.6 nH) required as high as six layers, yet the inductor density (with respect to footprint on the top layer) is >10 times lower, and at the same time SRF and Q are worse than those for the proposed advanced thick-film technology.

Table IV compares the reported highest achieved SRF (gigahertz) for similar value of inductance in various MCM technologies. When on Pimage-TF a 1.3 nH inductor provides an SRF of 15 GHz, then on LTCC (for 1.2 nH) and MLO (for 1.8 nH) provides SRF of 7.2 and 9.8 GHz, respectively. This reveals the superior performance and suitability of Pimage-TF technology for high frequency (millimeter-wave) MCM/SOP applications, where a required inductance can be realized within a much smaller foot-print (on top-layer) and with higher SRF. Furthermore, the presented results demonstrate that the circular spiral inductors can be realized on advanced ML Pimage-TF technology with high miniaturization, SRF, and inductor density, which are comparable with costlier thin-film technology [6], [20] and are better than most of the reported results in conventional thick-film-based MCM, including ceramic- based LTCC, laminate, LCP, and MLO technologies.

[19] G. Carchon, K. Vaesen, S. Brebels, W. De Raedt, E. Beyne, and B. Nauwelaers, "Multilayer thin-film MCM-D for the integration of high-performance RF and microwave circuits," *IEEE Trans. Compon. Packag. Manuf. Technol.*, vol. 24, no. 3, pp. 510–519, Sep. 2001.

[20] J.-H. Ko, S.-S. Ho, and Y.-S. Kwon, "Microshield transmission line and spiral inductor integrated on polymer thick film," in *IEEE MTT-S Dig.*, Jun. 2003, pp. 2281–2284.

Kamal K. Samanta (M'03–SM'08) received the double master's degrees in engineering (M.Tech.) and management (PGDOM), and the bachelor's degrees in physics (B.Sc.) and electronics engineering (B.Tech.). He received the B.Tech. and M.Tech. degrees from the Institute of Radiophysics and Electronics, University of Calcutta, Kolkata, India, and the Ph.D. degree from the Institute of Microwaves and Photonics, University of Leeds, Leeds, U.K.

He has been extensively involved in the industrial research, development, and manufacture of RF to millimeter-wave (mmW) (MHz to 180 GHz; CW power to MW) circuits and systems for about two decades. His roles have included that of Senior Principal/Principle Research and Development Engineer, Scientist, and Consultant. He was with Thales Aerospace and Defence, Crawley, U.K. (Radar/EW/ESM systems); European Aeronautics Defence and Space, Astrium, U.K. (GaN, HP, SatComm); Space Application Centre, Indian Space Research Organization, Ahmedabad, India [satellite payload Tx/Rx, monolithic microwave integrated circuits (MMICs)]; the Department of Atomic Energy, Institute for Plasma Research, Gandhinagar, India (2-MW, 64-phased array system for fusion reactor experiments); RFMD, Durham, U.K., and Filtronics Compound Semiconductor, Newton Aycliffe, U.K. (MMICs/radios). He is currently a Senior Principal Microwave Design Engineer and Project Manager with Milmega/AMETEK, Ryde, U.K., and a Visiting Researcher with the University of Leeds. His current research interests include development of novel microwave to sub-mmW circuits (MIC/MMIC, Si/GaAs/GaN, and PA), multilayer passives, cost-effective multichip modules, and system-on-package modules and technologies.

Dr. Samanta was a recipient of the Commonwealth Fellowship in 2003, the Best International Researcher Award, and the Engineering Excellence Award from the Institution of Engineering and Technology, London, in 2005 and 2006. He is a member of the Technical Program Committee of the IET and IEEE international conferences, sits on the Technical Committees of the IEEE Microwave Theory and Techniques Society (MTT-6, MTT-8, and MTT-12), and is also on the Editorial Board of the IEEE MICROWAVE AND WIRELESS COMPONENTS LETTERS and the *IET Microwaves, Antennas and Propagation*.

Ian D. Robertson (M'96–SM'05–F'12) was born in London, U.K., in 1963. He received the B.Sc. (Eng.) and Ph.D. degrees from King's College London, London, in 1984 and 1990, respectively.

He was with the Monolithic Microwave Integrated Circuit (MMIC) Research Group, Plessey Research, Caswell, U.K., from 1984 to 1986. He joined King's College London as a Research Assistant, Lecturer, and Reader, in 1994. In 1998, he became a Professor of Microwave Subsystems Engineering with the University of Surrey, Guildford, U.K., where he established the Microwave Systems Research Group and was a founding member of the Advanced Technology Institute. In 2004, he became the Centenary Chair in Microwave and Millimeter-Wave Circuits at the University of Leeds, Leeds, U.K., where he is currently the Head of the School of Electronic and Electrical Engineering. He has authored or co-authored over 400 papers in the areas of microwave integrated circuit and MMIC design. He edited the book entitled *MMIC Design* (IEE, 1995), and co-edited the book *RFIC & MMIC Design and Technology* [IEE, 2001 (in English) and Publishing House of Electronic Industry, 2007 (in Chinese)].

Dr. Robertson has organized many colloquia, workshops, and short courses for the Institution of Electrical Engineers (IEE) and IEEE. He was an Honorary Editor of *IEE Proceedings—Microwaves, Antennas, and Propagation* for many years and the Editor-in-Chief of the rebranded *IET Microwaves, Antennas and Propagation* from 2005 to 2009.

TABLE III

COMPARISON OF COMPACTNESS AND REPORTED HIGHEST INDUCTANCE IN ML MCM/SOP TECHNOLOGIES

Previous literatures and in this publication	*MCM Technology*	*No. of layers*	*Reported L(nH)*	*Foot-print on Surface layer (mm^2)*	*SRF (GHz)*	*f_{Qmax} (GHz)*	Q	*Compact. L/A (nH/mm^2)*
Ref.9	Laminate	2	22.2	2.364	2.58	-	11.06	9.4
Ref.8	LTCC	6	16.6	~12	1.6	0.8	41	1.3
Ref.3	LCP	2	4	--	8	2.4	70	--
Ref.7	Organic	2	10	1.29	4	1.3	65	7.75
Ref.7	Organic	2	15	--	3	0.6	35	--
Presented Work	Pimage-TF	1	30.5	1.69	2	1.2	31	15

TABLE IV

COMPARISON OF SRF (GIGAHERTZ) FOR INDUCTORS IN DIFFERENT CONVENTIONAL MCM TECHNOLOGIES

Previous literatures and in this publication	*MCM Technology*	*L (nH)*	*Turns (n)*	*Q*	*Highest SRF (GHz)*
Ref.9	Laminate	1.7	1	-	15
Ref.8	LTCC	1.2	3/4	100	7.2
Ref. 7	Organic (MLO)	1.8	1	65	9.8
Presented Work	Pimage-TF	1.3	1.5	82	20.5

V. CONCLUSION

A wide range of precisely defined embedded CPW circular spiral inductors have been developed, modeled, and characterized with remarkably high performance and up to a very high SRF and inductance density for thick-film-based cost-effective microwave and millimeter-wave MCM/SOP applications. The inductors are realized using a new and simplified layout generation technique with closed form expressions. The measured performances have been compared and shown to be better than most of the reported results in conventional thick-film-based MCM technologies, including MLO, laminate (MCM-L), and LTCC.

REFERENCES

[1] I. D. Robertson and S. Lucyszyn, *RFIC and MMIC Design and Technology*. London, U.K.: IET, 2001.

[2] H.-C. Lu, T. B. Chan, C. C. Chen, L. Chia-Ming, H.-J. Hsing, and P.-S. Huang, "LTCC spiral inductor synthesis and optimization with measurement verification," *IEEE Trans. Adv. Packag.*, vol. 33, no. 1, pp. 160–168, Feb. 2010.

[3] M. M. Tentzeris *et al.*, "3-D-integrated RF and millimeter-wave functions and modules using liquid crystal polymer (LCP) system-on-package technology," *IEEE Trans. Adv. Packag.*, vol. 27, no. 2, pp. 332–340, May 2004.

[4] M. F. Shafique and I. D. Robertson, "Laser prototyping of multilayer LTCC microwave components for system-in-package applications," *IET Microw. Antenna Propag.*, vol. 5, no. 8, pp. 864–869, Jun. 2011.

[5] K. K. Samanta, D. Stephens, and I. D. Robertson, "Design and performance of a 60-GHz multi-chip module receiver employing substrate integrated waveguides," *IEE Microw. Antenna Propag.*, vol. 1, no. 5, pp. 961–967, Oct. 2007.

[6] J. Y. Kim *et al.*, "V-band beam-steering ASK transmitter and receiver using BCB-based system-on-package technology on silicon mother board," *IEEE Microw. Wireless Compon. Lett.*, vol. 21, no. 11, pp. 619–621, Nov. 2011.

[7] H.-H. Lee and J.-Y. Park, "Characterisation of fully embedded RF inductors in organic SOP technology," *IEEE Trans. Adv. Packag.*, vol. 32, no. 2, pp. 491–496, Feb. 2010.

[8] A. Sutono, D. H. Heo, Y.-J. Chen, and J. Laskar, "High-Q LTCC-based passive library for wireless system-on-package (SOP) module development," *IEEE Trans. Microw. Theory Techn.*, vol. 49, no. 10, pp. 1715–1724, Oct. 2001.

[9] R. C. Lee, G.-A. Lee, and M. Megahed, "Design and analysis of embedded inductor on low cost multilayer laminate MCM technology," in *Proc. Elect. Perform. Electron. Packag.*, Oct. 2003, pp. 83–86.

[10] P. Pieters *et al.*, "Accurate modeling of high-Q spiral inductors in thin-film multilayer technology for wireless telecommunication applications," *IEEE Trans. Microw. Theory Techn.*, vol. 49, no. 4, pp. 589–599, Apr. 2001.

[11] K. K. Samanta and I. D. Robertson, "Advanced multilayer thick-film system-on-package technology for miniaturized and high performance CPW microwave passive components," *IEEE Trans. Compon. Packag. Manuf. Technol.*, vol. 1, no. 11, pp. 1695–1705, Nov. 2011.

[12] K. K. Samanta and I. D. Robertson, "Characterisation and application of embedded lumped elements in multilayer advanced thick-film multichip-module technology," *IET Microw., Antennas Propag.*, vol. 6, no. 1, pp. 52–59, Jan. 2012.

[13] K. K. Samanta, "Advanced multilayer photoimaged substrate integrated waveguides and RF front-end for emerging MM-wave wireless applications," in *Proc. IEEE WiSNet*, Newport Beach, CA, USA, Jan. 2014, pp. 16–18.

[14] K. K. Samanta, "Advanced photoimagable ceramic based technology: Substrate integrated waveguides and passives to multilayer cost-effective MCMs at MM-wave and beyond," in *Proc. IEEE MTT-S Int. Microw. RF Conf.*, New Delhi, India, Dec. 2013, pp. 1–4.

[15] K. K. Samanta and I. D. Robertson, "Dielectric thickness and ground-width effect on multilayer coplanar components and circuits for ceramic multichip modules," *Microw. Opt. Technol. Lett.*, vol. 54, no. 4, pp. 1127–1132, Mar. 2012.

[16] K. K. Samanta and I. D. Robertson, "Layout efficient and high performance circular spiral inductors for multilayer multichip modules," in *Proc. Eur. Microw. Conf.*, 2011, pp. 596–599.

[17] H. Okabe, H. Yamada, M. Yamasaki, O. Kagaya, K. Sekine, and K. Yamashita, "Characterization of a planar spiral inductor on a composite-resin low-impedance substrate and its application to microwave circuits," *IEEE Trans. Compon., Packag., Manuf. Technol., B, Adv. Packag.*, vol. 21, no. 3, pp. 269–273, Aug. 1998.

[18] A. Sutono, A. V.-H. Pham, J. Lasker, and W. R. Smith, "RF/microwave characterization of multilayer ceramic-based MCM technology," *IEEE Trans. Adv. Packag.*, vol. 22, no. 3, pp. 326–331, Aug. 1999.